

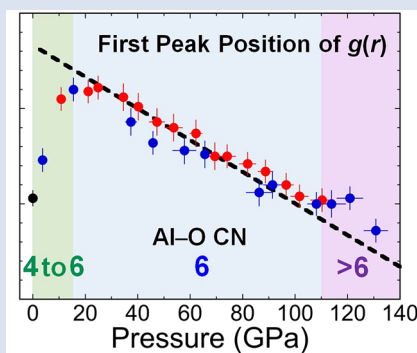
■ Ultrahigh pressure structural changes in a 60 mol. % Al_2O_3 –40 mol. % SiO_2 glass

I. Ohira^{1,2*}, Y. Kono^{1,3}, Y. Shibazaki^{4,5}, C. Kenney-Benson⁶, A. Masuno⁷, G. Shen⁶



doi: 10.7185/geochemlet.1913

Abstract



Structure of an Al-containing silicate glass (60 mol. % Al_2O_3 –40 mol. % SiO_2 , A40S) is investigated up to 131 GPa, a pressure close to that of the Earth's core-mantle boundary, by using our recently developed double stage large volume cell. The first peak (r_1) of the pair distribution function, which corresponds to T–O distance (T = Al, Si), rapidly increases below 16 GPa, indicating an increase of average coordination number (CN) of T–O from ~4 to 6. The r_1 linearly decreases in the pressure range of 25–110 GPa, but it displays a slope change and becomes nearly constant above 110 GPa. The slope change may imply a structural change in the A40S glass around 110 GPa, and may be explained by the change in Al–O distance associated with the Al–O CN increase from 6 to >6 as predicted by molecular dynamics simulations (Ghosh and Karki, 2018). Our observations suggest an important role for aluminum in densification of aluminosilicate at the deep lower mantle, which might imply a dense aluminosilicate magma with negative buoyancy.

Received 11 September 2018 | Accepted 26 March 2019 | Published 3 May 2019

Introduction

Pressure-induced structural change of silicate melts is one of the key factors in understanding the behaviour of silicate melts in the deep lower mantle to the core-mantle boundary (CMB), where the presence of silicate melt has been suggested by seismological studies as a cause of ultralow velocity zones (e.g., Garnero *et al.*, 1998). However, the structure of silicate melts at the ultrahigh pressure and high temperature conditions of the CMB is still poorly understood due to experimental challenges. Efforts have been made to understand pressure-induced structural changes in SiO_2 glass, considered an analogue of silicate melts. Murakami and Bass (2010) found a kink in the pressure dependence of the shear wave velocity (dv_s/dP) of a SiO_2 glass at 140 GPa, and proposed a possible ultrahigh pressure structural change with an increase of the average Si–O coordination number (CN) to >6. Sato and Funamori (2010) investigated the structure of SiO_2 glass and reported a constant Si–O CN of 6 from 35 GPa to 102 GPa. On the other hand, a recent structure measurement on SiO_2 glass up to 172 GPa showed a gradual increase of the average Si–O CN from 6 to higher than 6 above 50 GPa (Prescher *et al.*, 2017), while

the trend of the gradual increase of Si–O CN is different from a sharp structural change as the kink observed in the dv_s/dP (Murakami and Bass, 2010).

Kinks in dv_s/dP have also been observed in Al_2O_3 – SiO_2 glasses at 130 GPa (3.9 mol. % Al_2O_3 –96.1 mol. % SiO_2 glass) and at 116 GPa (20.5 mol. % Al_2O_3 –79.5 mol. % SiO_2 glass) (Ohira *et al.*, 2016). Ohira *et al.* (2016) suggested that incorporation of Al lowers the pressure condition of the ultrahigh pressure structural change, and indicated the role of aluminum in the structural change of aluminosilicate melts in the deep lower mantle. In fact, the composition of the melt generated by partial melting of a mid-ocean ridge basalt (MORB) at around 100 GPa contains a significant amount of Al_2O_3 (~20 wt. % or ~13 mol. %) (Pradhan *et al.*, 2015). Therefore, an understanding of the pressure-induced structural changes in aluminosilicate systems is important in determining the nature of such melts in the CMB region. However, direct structure measurements on aluminosilicate glasses have been limited to <30 GPa (e.g., Drewitt *et al.*, 2015), and pressure-induced structural changes of Al–O at the pressure condition in the deep lower mantle have not been experimentally studied. In this study, we experimentally determined the pair distribution functions of a 60

1. Geophysical Laboratory, Carnegie Institution of Washington, Argonne, IL 60439, USA
 2. Department of Earth and Planetary Materials Science, Graduate School of Science, Tohoku University, Sendai 980-8578, Japan
 3. Geodynamics Research Center, Ehime University, Ehime 790-8577, Japan
 4. Frontier Research Institute for Interdisciplinary Sciences, Tohoku University, Aoba-ku, Sendai 980-8578, Japan
 5. International Center for Young Scientists, National Institute for Materials Science, Tsukuba 305-0047, Japan
 6. High Pressure Collaborative Access Team, X-ray Science Division, Argonne National Laboratory, Argonne, IL 60439, USA
 7. Graduate School of Science and Technology, Hirosaki University, Hirosaki 036-8561, Japan
- * Corresponding author (email: itaru.ohira@gmail.com)



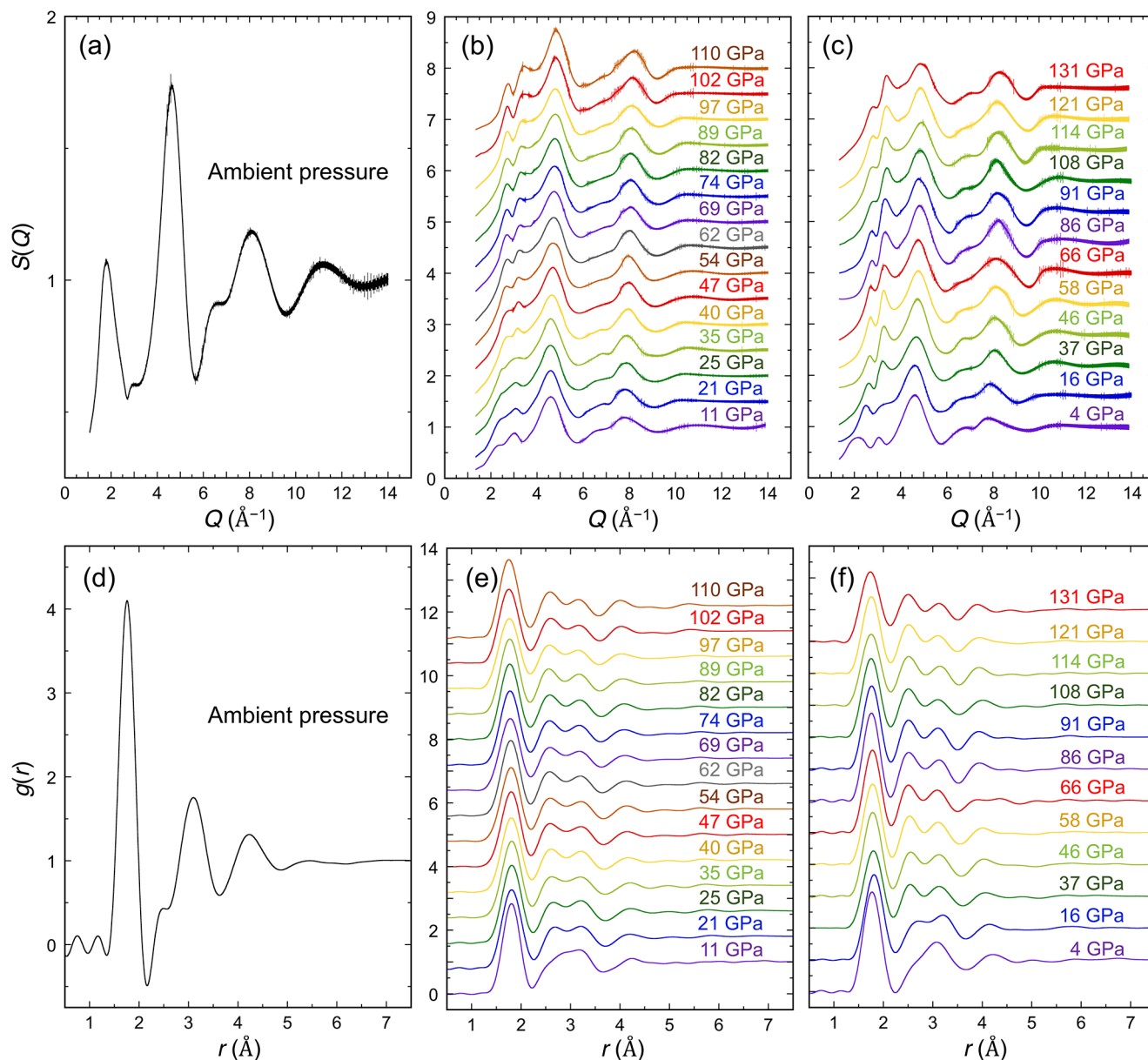


Figure 1 Structure factors, $S(Q)$, determined at the Q range up to 14 \AA^{-1} and pair distribution functions, $g(r)$, of the A40S glass up to 131 GPa. (a) $S(Q)$ at ambient condition. (b–c) $S(Q)$ at high pressures displayed by a vertical offset of 0.5 and 0.6 in (b) for experiment 1 and (c) for experiment 2, respectively. (d) $g(r)$ at ambient condition. (e–f) $g(r)$ at high pressures displayed by a vertical offset of 0.8 and 1.0 in (e) for experiment 1 and (f) for experiment 2, respectively.

mol. % Al_2O_3 –40 mol. % SiO_2 glass (hereafter A40S glass) up to 131 GPa, and found an ultrahigh pressure structural change in this glass at pressures above 110 GPa.

Structure Measurement up to 131 GPa

Figure 1 shows structure factors, $S(Q)$, of the A40S glass up to 131 GPa (Fig. 1a–c), and the reduced pair distribution functions, $g(r)$ (Fig. 1d–f). The first peak (r_1) of $g(r)$ is considered to represent the T–O (T = Al and Si) distance. Since Si–O and Al–O bond distances are very close (for example, 1.64 \AA and 1.81 \AA , respectively, in $\text{CaAl}_2\text{Si}_2\text{O}_8$ glass calculated by Ghosh and Karki, 2018), these bond distances are not resolvable even in the measurements at ambient pressure (e.g., Okuno *et al.*, 2005; Ohira *et al.*, 2016). Our observed r_1 at ambient pressure ($1.753 \pm 0.004 \text{ \AA}$) is consistent with that reported in a previous ambient pressure study ($1.76 \pm 0.01 \text{ \AA}$ with T–O CN of 4.3 ± 0.1 ; Okuno *et al.*, 2005). At ambient pressure, we observed that

there is a single second peak at $\sim 3.1 \text{ \AA}$ with a shoulder peak at $\sim 2.5 \text{ \AA}$, while it changes to two distinct peaks above 16 GPa (r_2 at ~ 2.5 – 2.6 \AA and r_3 at ~ 3.1 – 3.2 \AA). The basic feature of $g(r)$ in the A40S glass above 16 GPa is similar to that of SiO_2 glass with 6-fold coordinated structure at high pressures (Sato and Funamori, 2010; Prescher *et al.*, 2017), while the peak positions are different due to the difference between the Al–O and Si–O distances.

Figure 2 shows pressure dependences of r_1 , r_2 , and r_3 of the A40S glass, with the numerical data summarised in Table 1. r_1 rapidly increases with increasing pressure at pressures below 16 GPa, and then almost linearly decreases with increasing pressure in the pressure range between 25 and 102 GPa (Fig. 2a). The slope of r_1 changes with pressure at 25–102 GPa is similar to those of the Si–O bond distance in SiO_2 glass with Si–O CN of ~ 6 at 35–102 GPa (Sato and Funamori, 2010) and Al–O bond distance in $\text{CaAl}_2\text{Si}_2\text{O}_8$ glass with Al–O CN of ~ 6 at 41–105 GPa (Ghosh and Karki, 2018) (Fig. 2a). We find that r_1 starts to deviate from the linear compression

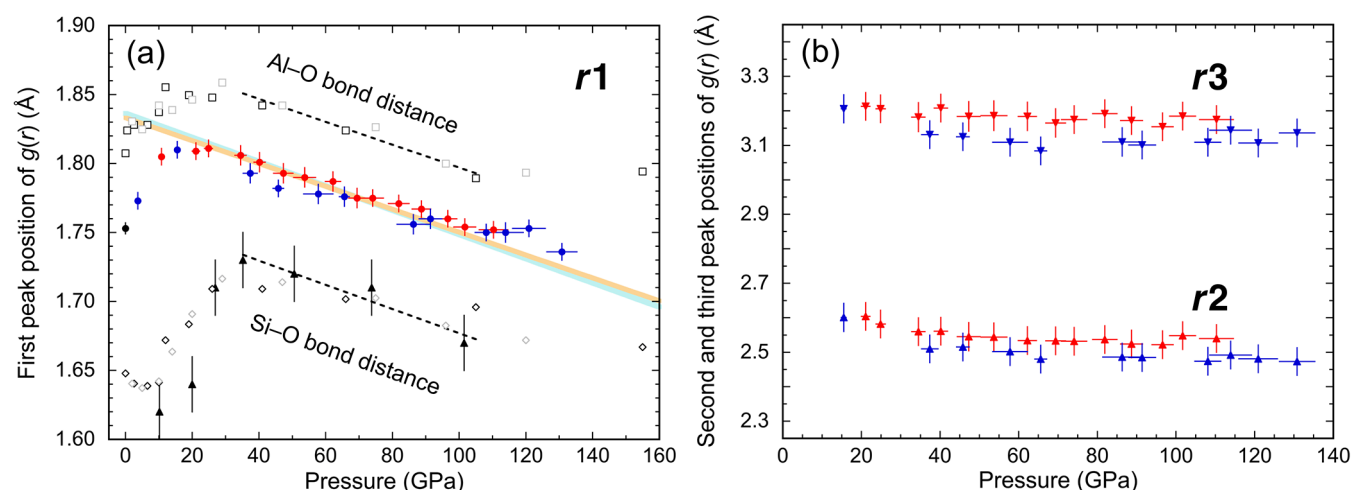


Figure 2 The first (r_1), second (r_2), and third (r_3) peak positions of $g(r)$ of the A40S glass. (a) Red, blue, and black circles indicate the r_1 determined in the high pressure experiments 1 and 2, and at ambient pressure, respectively. Triangles indicate the Si–O bond distance in SiO₂ glass (Sato and Funamori, 2010). Open diamonds and squares indicate the Si–O and Al–O bond distance in CaAl₂Si₂O₈ glass, respectively, simulated with 416 (black) and 208 (gray) atom simulation cells (Ghosh and Karki, 2018). The black dash lines are obtained from fitting for the Si–O and Al–O bond distances with CN = ~6. The light blue and orange lines are obtained from fitting the r_1 of A40S glass at 35–102 GPa using the $dr_{\text{Si-O}(6\text{CN})}/dP$ and the $dr_{\text{Al-O}(6\text{CN})}/dP$, respectively. The widths of lines indicate the fitting errors. (b) The r_2 and r_3 of the A40S glass determined in the experiments 1 (red) and 2 (blue), respectively.

trend above ~110 GPa and becomes constant at 110–121 GPa (Fig. 2a). The determined r_2 and r_3 values show some differences between the two experiments (up to 0.1 Å), while these are almost within the experimental errors. It is noted, however, that the experimental results from both runs show monotonous changes in r_2 and r_3 between 16 and 131 GPa (Fig. 2b).

Table 1 Experimental pressure conditions and the first (r_1), second (r_2), and third (r_3) peak positions of $g(r)$.

Pressure (GPa)	r_1 (Å)	r_2 (Å)	r_3 (Å)
Ambient 0.0001	1.753 ± 0.004		
Experiment 1			
10.8 ± 0.7	1.805 ± 0.006		
21.1 ± 1.1	1.809 ± 0.006	2.604 ± 0.040	3.213 ± 0.040
24.9 ± 1.2	1.811 ± 0.006	2.582 ± 0.040	3.206 ± 0.040
34.5 ± 1.7	1.806 ± 0.007	2.560 ± 0.040	3.182 ± 0.042
40.2 ± 1.7	1.801 ± 0.007	2.561 ± 0.040	3.208 ± 0.040
47.3 ± 2.9	1.793 ± 0.007	2.545 ± 0.041	3.184 ± 0.043
53.7 ± 3.3	1.790 ± 0.007	2.544 ± 0.041	3.186 ± 0.043
62.2 ± 2.3	1.787 ± 0.007	2.534 ± 0.040	3.184 ± 0.041
69.4 ± 2.5	1.775 ± 0.007	2.533 ± 0.040	3.165 ± 0.041
74.1 ± 3.2	1.775 ± 0.006	2.532 ± 0.040	3.175 ± 0.040
81.9 ± 3.1	1.771 ± 0.006	2.537 ± 0.040	3.192 ± 0.040
88.7 ± 2.8	1.767 ± 0.006	2.524 ± 0.040	3.172 ± 0.040
96.6 ± 2.7	1.760 ± 0.006	2.522 ± 0.040	3.154 ± 0.040
101.7 ± 3.3	1.754 ± 0.006	2.548 ± 0.040	3.185 ± 0.040
110.3 ± 4.3	1.752 ± 0.006	2.540 ± 0.040	3.175 ± 0.040
Experiment 2			
3.7 ± 0.3	1.773 ± 0.006		
15.5 ± 0.6	1.810 ± 0.006	2.601 ± 0.041	3.206 ± 0.041
37.4 ± 2.1	1.793 ± 0.007	2.510 ± 0.040	3.131 ± 0.040
45.8 ± 1.6	1.782 ± 0.006	2.515 ± 0.040	3.125 ± 0.040
57.8 ± 4.4	1.778 ± 0.007	2.502 ± 0.040	3.109 ± 0.040
65.6 ± 1.5	1.776 ± 0.007	2.480 ± 0.040	3.084 ± 0.040
86.3 ± 4.9	1.756 ± 0.007	2.486 ± 0.040	3.110 ± 0.041
91.4 ± 3.4	1.760 ± 0.007	2.485 ± 0.040	3.101 ± 0.040
108.1 ± 3.3	1.750 ± 0.006	2.474 ± 0.040	3.109 ± 0.040
113.9 ± 5.3	1.750 ± 0.007	2.492 ± 0.040	3.144 ± 0.040
120.9 ± 4.3	1.753 ± 0.006	2.481 ± 0.040	3.107 ± 0.040
130.8 ± 4.5	1.736 ± 0.006	2.473 ± 0.040	3.136 ± 0.040

Discussion

The A40S glass has a significantly higher content of Al than Si (Al/Si = 3), and therefore the behaviour of r_1 is considered to mainly represent the Al–O distance. In fact, our observed behaviour of r_1 at low pressure (<25 GPa) is consistent with the behaviour of Al–O distance reported in previous studies. Drewitt *et al.* (2015) showed an increase in Al–O distance in CaAl₂O₄ glass with increasing pressure below 15 GPa, and then it displayed a slight decrease above 15 GPa. Along with the increase in Al–O distance, the average Al–O CN of CaAl₂O₄ glass increases from 4 at ambient pressure to 6 at ~23.5 GPa (Drewitt *et al.*, 2015). In addition, a recent simulation study for CaAl₂Si₂O₈ glass found that the Al–O distance increases with increasing pressure below ~20 GPa together with an increase of average Al–O CN (Ghosh and Karki, 2018) (Fig. 2a). The behaviour of the Al–O distance experimentally determined by Drewitt *et al.* (2015) and calculated by Ghosh and Karki (2018) is consistent with the change in r_1 of the A40S glass obtained in this study (Fig. 2a). The increase of r_1 below 16 GPa here is considered to represent an increase of Al–O CN from ~4 to 6. The pressure condition where the Al–O CN reaches 6 is markedly lower than the pressure where the Si–O CN in SiO₂ glass reaches 6 (at ~35–50 GPa: Sato and Funamori, 2010; Prescher *et al.*, 2017). Contrary to the behaviour of Al–O distance, Si–O distance decreases with increasing pressure up to ~10–20 GPa and then increases at ~20–35 GPa (Sato and Funamori, 2010; Ghosh and Karki, 2018) (Fig. 2a), which is markedly different from our observed r_1 .

Above 25 GPa, r_1 linearly decreases with increasing pressure, while it starts to deviate from a linear trend above around 110 GPa (Fig. 2a), which implies an existence of another structural change under ultrahigh pressure conditions. We find that the slope of the r_1 changes in the A40S glass at 25–102 GPa shows a trend similar to the behaviour of Si–O and Al–O bond distances in SiO₂ glass (Sato and Funamori, 2010) and CaAl₂Si₂O₈ glass (Ghosh and Karki, 2018) with 6-fold coordinated structure, respectively. The Si–O bond distance shows a linear compression slope of $dr_{\text{Si-O}(6\text{CN})}/dP = -8.77 \times 10^{-4}$ Å/GPa at 35–102 GPa (Fig. 2a). Similarly, the Al–O bond distance shows a slope of $dr_{\text{Al-O}(6\text{CN})}/dP$ of -8.30×10^{-4} Å/GPa (Fig. 2a), which is almost identical to the slope of Si–O. We therefore consider that the slope of the T–O bond distance (T = Si, Al)

with T–O CN of 6 in the A40S glass can be expressed by the same dr_1/dP as those of Si–O and Al–O bond distances. Indeed, when the r_1 values are plotted with slopes of dr_1/dP being $-8.77 \times 10^{-4} \text{ \AA/GPa}$ and $-8.30 \times 10^{-4} \text{ \AA/GPa}$ at 34.5–101.7 GPa for SiO₂ and CaAl₂Si₂O₈ glasses, respectively, it appears that the behaviour of r_1 in the A40S glass below 110 GPa can be well explained by the dr_1/dP slopes of the 6-fold coordinated structure. Above 110 GPa, however, r_1 values deviate from the linear trends (Fig. 2a). Even if the linear range is selected at different pressure ranges (for example, at 35–131 GPa) or used for individual runs in experiment 1 and 2, the deviation of r_1 from linear trends above 110 GPa can still be clearly identified (Fig. S-1). These results suggest a structural change at short range scale at ultrahigh pressures above ~110 GPa.

The kink in r_1 of the A40S glass at 110 GPa in this study is consistent with the behaviour of Al–O distance in CaAl₂Si₂O₈ glass reported by Ghosh and Karki (2018). Ghosh and Karki (2018) showed a decrease of Al–O distance between ~10 and ~110 GPa, while it becomes constant or slightly increases above ~110 GPa in CaAl₂Si₂O₈ glass. The average Al–O CN of CaAl₂Si₂O₈ glass is constant at around 6 in a pressure range between 41 and 105 GPa, while it starts to increase to >6 above ~110 GPa (Ghosh and Karki, 2018). Thus, the kink in the pressure dependence of Al–O distance in CaAl₂Si₂O₈ glass at ~110 GPa is considered to represent the average Al–O CN increase from 6 to >6 (Ghosh and Karki, 2018). Although it is difficult for us to determine the average T–O CN in our A40S glass because of the lack of available density data for the A40S glass, the similarity between the Al–O distance change in Ghosh and Karki (2018) and the change in r_1 in this study suggests an ultrahigh pressure structural change in the A40S glass to a more than 6-fold coordinated Al–O structure above 110 GPa. While r_1 is nearly constant at 110–121 GPa, there is a decrease in r_1 at 121–131 GPa. This decrease of r_1 may imply that the change of Al–O CN may be completed at 131 GPa, in contrast to the theoretical prediction of a continuous Al–O CN increase to at least 155 GPa (Ghosh and Karki, 2018). However, data points are still limited, and further structural measurements at higher pressures are required to understand this question better. In addition, our observed decrease in r_1 may be influenced by Si–O bond of the A40S glass, since the evolution of Si–O CN is still controversial in literature (for example, a gradual increase of Si–O CN to more than 6 above 50 GPa in Prescher *et al.*, 2017, while Si–O CN of less than 6 up to 155 GPa in Ghosh and Karki, 2018).

The pressure condition of the ultrahigh pressure structural change in the A40S glass observed in this study (110 GPa) is similar to the pressure condition where a kink in dv_S/dP is observed for Al₂O₃–SiO₂ glasses (116 GPa for 20.5 mol. % Al₂O₃–79.5 mol. % SiO₂ glass, Ohira *et al.*, 2016). The data suggest that the kink in the dv_S/dP is attributable to the increase of average Al–O CN to >6. Ohira *et al.* (2016) argued that incorporation of Al decreases the pressure of the sound velocity change of Al₂O₃–SiO₂ glasses. Therefore, the ultrahigh pressure structural change to more than 6-fold coordinated structure in Al₂O₃–SiO₂ system may also depend on the ratio of Si and Al.

The pressure condition of the Al–O CN change at 110 GPa is shallower than that of the CMB. Considering the similarity in the pressure-induced structural changes between aluminosilicate glass and melt at very high pressure conditions of the Earth's lower mantle (Sanloup, 2016), the Al–O CN change may occur in aluminosilicate melt in the CMB region and may have a significant influence on the behaviour of Al-rich aluminosilicate magmas generated by partial melting of MORB (Pradhan *et al.*, 2015). It is interesting to note that Al-rich glasses show different behaviour in density from those of Al-free silicate glasses. Petitgirard *et al.* (2015, 2017)

showed a similarity in density of SiO₂ and MgSiO₃ glasses at the pressure conditions of the Earth's lowermost mantle, which indicates a minor effect of SiO₂ content on the density of silicate glasses (Fig. S-2). On the other hand, we note that the density of CaAl₂Si₂O₈ glass (Ghosh and Karki, 2018) becomes higher than those of SiO₂ and MgSiO₃ glasses above 82 and 64 GPa, respectively (Fig. S-2), likely due to an average Al–O CN change to >6 while the average Si–O CN remains at 6. It has been known that densities of SiO₂ and MgSiO₃ glasses are lower than that of the Preliminary reference Earth model (PREM) (Dziewonski and Anderson, 1981) at the pressures of the CMB (Petitgirard *et al.*, 2017). The important role of Fe in the formation of silicate magma with density higher than PREM has been discussed in previous studies (*e.g.*, Petitgirard *et al.*, 2015, 2017; Karki *et al.*, 2018). A recent study showed that only highly Fe-rich melts (*e.g.*, ~0.35 of Fe/(Mg+Fe)) could be denser than the surrounding mantle (Karki *et al.*, 2018). However, to generate such a Fe-rich melt, very low partition coefficients ($D_{\text{Fe}}^{\text{mineral/melt}}$) and low degree of partial melting are required (*e.g.*, Andrault *et al.*, 2017), while these parameters at ultrahigh pressure and high temperature conditions of the deep lower mantle are still under debate (*e.g.*, Andrault *et al.*, 2017). On the other hand, Fe-free CaAl₂Si₂O₈ glass has markedly higher density than SiO₂ and MgSiO₃ glasses above 100 GPa (Fig. S-2), which suggests an important densification role of average Al–O CN to more than 6 in the formation of dense magma at pressures near the CMB.

Acknowledgements

We are grateful to the three anonymous reviewers for their comments that helped to improve the manuscript. High pressure experiments were performed at HPCAT (Sector 16), Advanced Photon Source (APS), Argonne National Laboratory. HPCAT operation is supported by DOE–NNSA under Award No. DE-NA0001974. The Advanced Photon Source is a U.S. Department of Energy (DOE) Office of Science User Facility operated for the DOE Office of Science by Argonne National Laboratory under Contract No. DE-AC02-06CH11357. This research is supported by JSPS overseas fellowships to IO and the National Science Foundation under Award No. EAR-1722495 to YK. GS acknowledges the support of DOE-BES/DMSE under Award DE-FG02-99ER45775. YS acknowledges the support of JSPS KAKENHI Grant Number 15K17784.

Editor: Wendy Mao

Additional Information

Supplementary Information accompanies this letter at <http://www.geochemicalperspectivesletters.org/article1913>.



This work is distributed under the Creative Commons Attribution Non-Commercial No-Derivatives 4.0 License, which permits unrestricted distribution provided the original author and source are credited. The material may not be adapted (remixed, transformed or built upon) or used for commercial purposes without written permission from the author. Additional information is available at <http://www.geochemicalperspectivesletters.org/copyright-and-permissions>.

Cite this letter as: Ohira, I., Kono, Y., Shibazaki, Y., Kenney-Benson, C., Masuno, A., Shen, G. (2019) Ultrahigh pressure structural changes in a 60 mol. % Al₂O₃–40 mol. % SiO₂ glass. *Geochem. Persp. Let.* 10, 41–45.



References

- ANDRAULT, D., BOLEFAN-CASANOVA, N., BOUHIFD, M.A., BOUJIBAR, A., GARBARINO, G., MANTHILAKE, G., MEZOUAR, M., MONTEUX, J., PARISIADIS, P., PESCE, G. (2017) Toward a coherent model for the melting behavior of the deep Earth's mantle. *Physics of the Earth and Planetary Interiors* 265, 67–81.
- DREWITT, J.W.E., JAHN, S., SANLOUP, C., DE GROUCHY, C., GARBARINO, G., HENNET, L. (2015) Development of chemical and topological structure in aluminosilicate liquids and glasses at high pressure. *Journal of Physics: Condensed Matter* 27, 105103.
- DZIEWONSKI, A.M., ANDERSON, D.L. (1981) Preliminary reference Earth model. *Physics of the Earth and Planetary Interiors* 25, 297–356.
- GARNERO, E.J., REVENAUGH, J., WILLIAMS, Q., LAY, T., KELLOGG, L.H. (1998) Ultralow velocity zone at the core-mantle boundary. In: Gurnis, M., Wyssession, M.E., Knittle, E., Buffett, B.A. (Eds.) *The core-mantle boundary region*. The American Geophysical Union, Washington, D.C., 319–334.
- GHOSH, D.B., KARKI, B.B. (2018) First-principles molecular dynamics simulations of anorthite (CaAl₂Si₂O₈) glass at high pressure. *Physics and Chemistry of Minerals* 45, 575–587.
- KARKI, B.B., GHOSH, D.B., MAHARJAN, C., KARATO, S.-I., PARK, J. (2018) Density-pressure profiles of Fe-bearing MgSiO₃ liquid: effects of valence and spin states, and implications for the chemical evolution of the lower mantle. *Geophysical Research Letters* 45, 3959–3966.
- MURAKAMI, M., BASS, J.D. (2010) Spectroscopic evidence for ultrahigh-pressure polymorphism in SiO₂ glass. *Physical Review Letters* 104, 025504.
- OHIRA, I., MURAKAMI, M., KOHARA, S., OHARA, K., OHTANI, E. (2016) Ultrahigh-pressure acoustic wave velocities of SiO₂-Al₂O₃ glasses up to 200 GPa. *Progress in Earth and Planetary Science* 3, 18.
- OKUNO, M., ZOTOV, N., SCHMÜCKER, M., SCHNEIDER, H. (2005) Structure of SiO₂-Al₂O₃ glasses: combined X-ray diffraction, IR and Raman studies. *Journal of Non-Crystalline Solids* 351, 1032–1038.
- PETITGIRARD, S., MALFAIT, W.J., SINMYO, R., KUPENKO, I., HENNET, L., HARRIES, D., DANE, T., BURGHAMMER, M., RUBIE, D.C. (2015) Fate of MgSiO₃ melts at core-mantle boundary conditions. *Proceedings of the National Academy of Sciences of the United States of America* 112, 14186–14190.
- PETITGIRARD, S., MALFAIT, W.J., JOURNAUX, B., COLLINGS, I.E., JENNINGS, E.S., BLANCHARD, I., KANTOR, I., KURNOSOV, A., COTTE, M., DANE, T., BURGHAMMER, M., RUBIE, D.C. (2017) SiO₂ glass density to lower-mantle pressures. *Physical Review Letters* 119, 215701.
- PRADHAN, G.K., FIQUET, G., SIEBERT, J., AUZENDE, A.-L., MORARD, G., ANTONANGELI, D., GARBARINO, G. (2015) Melting of MORB at core-mantle boundary. *Earth and Planetary Science Letters* 431, 247–255.
- PRESCHER, C., PRAKAPENKA, V.B., STEFANSKI, J., JAHN, S., SKINNER, L.B., WANG, Y. (2017) Beyond sixfold coordinated Si in SiO₂ glass at ultrahigh pressures. *Proceedings of the National Academy of Sciences of the United States of America* 114, 10041–10046.
- SANLOUP, C. (2016) Density of magmas at depth. *Chemical Geology* 429, 51–59.
- SATO, T., FUNAMORI, N. (2010) High-pressure structural transformation of SiO₂ glass up to 100 GPa. *Physical Review B* 82, 184102.